Mass spectrometric identification of intermediates in the O_2-driven [4Fe-4S] to [2Fe-2S] cluster conversion in FNR

Jason C. Crack[a], Andrew J. Thomson[a], and Nick E. Le Brun[a,1]

[a]Centre for Molecular and Structural Biochemistry, School of Chemistry, University of East Anglia, Norwich Research Park, Norwich NR4 7TJ, United Kingdom

Edited by Dennis R. Dean, Virginia Polytechnic Institute, Blacksburg, Virginia, and accepted by Editorial Board Member Michael A. Marletta March 7, 2017 (received for review December 21, 2016)

The iron-sulfur cluster containing protein Fumarate and Nitrate Reduction (FNR) is the master regulator for the switch between anaerobic and aerobic respiration in *Escherichia coli* and many other bacteria. The [4Fe-4S] cluster functions as the sensory module, undergoing reaction with O_2 that leads to conversion to a [2Fe-2S] form with loss of high-affinity DNA binding. Here, we report studies of the FNR cluster conversion reaction using time-resolved electrospray ionization mass spectrometry. The data provide insight into the reaction, permitting the detection of cluster conversion intermediates and products, including a [3Fe-3S] cluster and persulfide-coordinated [2Fe-2S] clusters [$[2Fe\text{-}2S](S)_n$, where $n = 1$ or 2]. Analysis of kinetic data revealed a branched mechanism in which cluster sulfide oxidation occurs in parallel with cluster conversion and not as a subsequent, secondary reaction to generate $[2Fe\text{-}2S](S)_n$ species. This methodology shows great potential for broad application to studies of protein cofactor–small molecule interactions.

iron-sulfur | mass spectrometry | oxygen sensor | DNA regulation

A remarkable feature of bacteria is their ability to adapt to rapidly changing environments. Many bacterial species, including the model organism *Escherichia coli*, are capable of growth on a variety of substrates under varying oxygen tensions. In the absence of O_2, alternative electron acceptors, such as fumarate or nitrate, are used to support growth (1). However, these alternative metabolic pathways are less efficient than aerobic respiration. Therefore, the ability to monitor the availability of O_2 and respond by reprogramming gene expression is necessary for these bacteria to remain competitive.

In *E. coli* and many other bacteria, the O_2-sensing Fumarate and Nitrate Reduction (FNR) protein is the master regulator of the switch between aerobic and anaerobic metabolism (2–5). The first crystal structure of dimeric holo-FNR, from *Aliivibrio fischeri*, was recently reported (6). AfFNR is the same length as and shares 84% sequence identity with *E. coli* FNR. Like other members of the cAMP receptor protein superfamily, FNR comprises two distinct domains, providing sensory and DNA binding functions linked by a dimer interface (Fig. 1*A*). The N-terminal sensory domain contains four essential Cys residues (Cys20, -23, -29, and -122) (7–9) that are capable of binding either a $[4Fe\text{-}4S]^{2+}$ (Fig. 1*B*) or a $[2Fe\text{-}2S]^{2+}$ cluster. The C-terminal DNA binding domain recognizes specific FNR binding sequences within target promoters. In the absence of O_2, monomeric (~30 kDa) FNR acquires a $[4Fe\text{-}4S]^{2+}$ cluster, triggering a conformational change at the dimerization interface that leads to the formation of homodimers (~60 kDa) and site-specific DNA binding (10, 11). Kiley and coworkers (8, 12) established that the $[4Fe\text{-}4S]^{2+}$ EcFNR is converted into a $[2Fe\text{-}2S]^{2+}$ form both in vivo and in vitro and that this results in a rearrangement of the dimer interface, leading to monomerization (10).

Through a combination of visible absorbance and EPR spectroscopies, we identified an EPR active $[3Fe\text{-}4S]^{1+}$ ($S = 1/2$) species as a transient intermediate in the cluster conversion process, indicating a two-step process (**1** and **2**) (13, 14):

$$\textbf{Step 1}: [4Fe\text{-}4S]^{2+} + O_2 \rightarrow [3Fe\text{-}4S]^{1+} + Fe^{2+} + O_2^{-}, \quad [1]$$

$$\textbf{Step 2}: [3Fe\text{-}4S]^{1+} \rightarrow [2Fe\text{-}2S]^{2+} + Fe^{3+} + 2S^{2-}. \quad [2]$$

In step 1, an Fe^{2+} ion is released to generate the $[3Fe\text{-}4S]^{1+}$ intermediate. This release likely occurs after one-electron oxidation of the $[4Fe\text{-}4S]^{2+}$ cluster to yield an unstable $[4Fe\text{-}4S]^{3+}$ cluster that ejects Fe^{2+}. Step 2 corresponds to the conversion of the $[3Fe\text{-}4S]^{1+}$ species to the $[2Fe\text{-}2S]^{2+}$ cluster. Although two sulfide ions are released from the cluster during the $[4Fe\text{-}4S]^{2+}$ to $[2Fe\text{-}2S]^{2+}$ cluster conversion (15), how this happens is unknown. They may be ejected into aqueous solution or undergo two-electron oxidation to form sulfane (S^0), which subsequently reacts with Cys side chains (RS^-) to form persulfides (RSS^-). The latter can serve as ligands to the [2Fe-2S] cluster as recently shown (16, 17). Similarly, liquid chromatography mass spectrometry (LC-MS) experiments showed that multiple cysteine persulfides $[RS(S)_n$, where $n = 1$–4] were formed during the FNR reaction time course (16). Step 2 may thus also be O_2-dependent and, hence, more complex than initially envisaged (**3** and **4**):

$$\textbf{Step 2}: \textbf{One persulfide ligated } [\mathbf{2Fe-2S}]$$
$$[3Fe\text{-}4S](RS)_3 + RS^- + O_2 + 2H^+ \rightarrow [2Fe\text{-}2S](RS)_3(RSS) + Fe^{3+} + S^{2-} + H_2O_2 \quad [3]$$

Significance

The transcriptional regulator Fumarate and Nitrate Reduction is the master switch for the transition between anaerobic and aerobic respiration in many other bacteria. It fulfills this role by controlling the expression of >300 genes in response to O_2. It senses O_2 through a [4Fe-4S] cluster cofactor, which undergoes conversion to a [2Fe-2S] cluster on reaction with O_2, leading to loss of DNA binding. By using time-resolved electrospray ionization mass spectrometry, we gained insight into the reaction through detection of cluster conversion intermediates and products, including a [3Fe-3S] cluster. The data also show that sulfide released from the cluster is oxidized during the conversion reaction and not after it. Our methodology has great potential for broad application to studies of cofactor reactivities.

Author contributions: J.C.C., A.J.T., and N.E.L.B. designed research; J.C.C. performed research; J.C.C. and N.E.L.B. analyzed data; and A.J.T. and N.E.L.B. wrote the paper.

The authors declare no conflict of interest.

This article is a PNAS Direct Submission. D.R.D. is a Guest Editor invited by the Editorial Board.

[1]To whom correspondence should be addressed. Email: n.le-brun@uea.ac.uk.

This article contains supporting information online at www.pnas.org/lookup/suppl/doi:10.1073/pnas.1620987114/-/DCSupplemental.

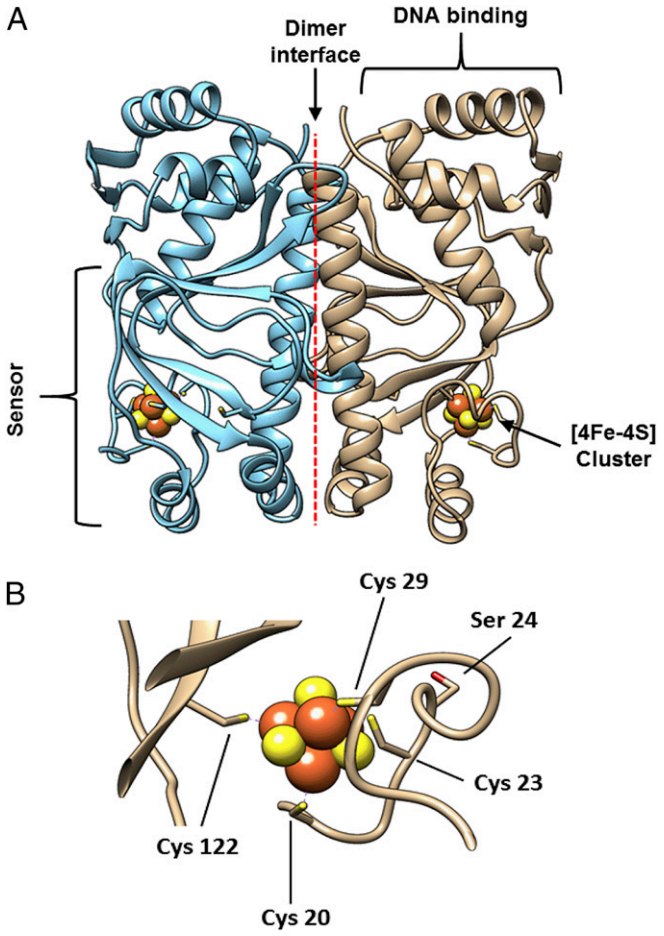

Fig. 1. Crystal structure of FNR from *A. fischeri*. (*A*) AfFNR is a homodimer composed of monomeric subunits (blue and brown). Each subunit binds an all cysteine-ligated [4Fe-4S] cluster (shown as space filled) and contains an N-terminal sensory domain, a C-terminal DNA binding domain, and a large dimerization helix that forms the dimer interface. (*B*) The [4Fe-4S] cluster binding loop of AfFNR (Protein Bata Dank ID code 5E44). The location of Ser24 is shown relative to the positions of the cluster ligands (Cys20, -23, -29, and -122).

or

$$\textbf{Step 2 : Two persulfide ligated}[\mathbf{2Fe-2S}]$$
$$[3\text{Fe-}4\text{S}](\text{RS})_3 + \text{RS}^- + \text{O}_2 + 4\text{H}^+ \rightarrow [2\text{Fe-}2\text{S}](\text{RS})_2(\text{RSS})_2 + \text{Fe}^{3+} + 2\text{H}_2\text{O}. \quad [4]$$

A persulfide-coordinated [2Fe-2S] cluster may serve to retain sulfur that can be used for conversion back to the original [4Fe-4S] form. This process was shown on addition of a reductant (to reduce sulfane back to sulfide) plus Fe^{2+}. This reversibility points to a pathway for iron-sulfur cluster repair that does not need to involve Fe-S biogenesis machinery (16). The complexity of the [3Fe-4S] to [2Fe-2S] conversion process means that it probably involves more than one reaction. Additional complexity arises depending on whether sulfide oxidation occurs simultaneously with iron release or after it.

Here we report time-resolved electrospray ionization mass spectrometry (ESI-MS) of *E. coli* FNR in response to its physiologically relevant analyte, O_2. This methodology couples soft ESI and TOF detection with solution and ionization conditions under which proteins remain folded (18, 19). This experimental approach enables accurate mass detection of intact folded proteins and protein complexes and has already been used extensively to study protein–protein interactions and the interactions of proteins with other molecules (20, 21) as well as protein structural changes (19, 22). ESI-MS of metalloproteins, where the metal cofactor remains bound after vaporization/ionization, has also been shown to be a valuable technique for the study of metalloproteins (23–25), including iron-sulfur proteins (26, 27), but still remains relatively underexploited given its potential to provide significant insight into the chemistry taking place at metal cofactor active sites.

For this study, we have used the S24F variant of FNR, which undergoes the same cluster conversion reaction as the WT protein but at a significantly reduced rate (28), thus facilitating analysis by ESI-MS. The data provide an unusually detailed view of the cluster conversion process, revealing the formation of a [3Fe-3S] protein-bound intermediate and the oxidation of cluster sulfide during cluster conversion.

Results

Detection of [4Fe-4S] FNR by ESI-MS. ESI-MS was used to detect [4Fe-4S] S24F FNR (hereafter referred to as FNR). The *m/z* spectrum (Fig. 2*A*) has three distinct regions corresponding to monomeric [4Fe-4S] FNR (1,000–2,500 *m/z*), monomeric apo-FNR containing multiple sulfur adducts (2,300–3,100 *m/z*), and dimeric [4Fe-4S] FNR (3,000–4,500 *m/z*). The deconvoluted spectrum of [4Fe-4S] FNR (Fig. S1*A*) revealed a major species at 29,898 Da caused by monomeric [4Fe-4S] FNR (predicted mass of 29,897 Da) (Table 1 shows a list of observed and predicted masses). A number of low-intensity, poorly resolved features were also observed to the higher mass side of [4Fe-4S] FNR, the clearest of which was at +40 Da. This peak was also present in LC-MS spectra, indicating that it arises from a small proportion of the protein that is covalently modified in some way (Fig. S2). In the lower-mass region, a minor peak was observed at 29,545 Da, corresponding to apo-FNR (predicted mass of 29,547 Da), with a 2-Da shift possibly caused by a single disulfide bond. More intense peaks were also observed at 29,609 and 29,673 Da, corresponding to two and four sulfur adducts of apo-FNR (+64 and +128 Da), respectively. Appreciable amounts of [2Fe-2S] FNR at 29,720 Da (predicted mass of 29,721 Da) were detected in some samples, indicative of a small amount of O_2-mediated damage. Optimization of ionization conditions to favor the detection of the monomeric form of [4Fe-4S] FNR resulted in *m/z* and deconvoluted spectra (Fig. 2*B* and Fig. S1*B*) dominated by [4Fe-4S] FNR, with significantly less (<12%) of the lower mass forms of FNR.

Because [4Fe-4S] FNR is a dimer in solution, the observation of monomer [4Fe-4S] FNR suggests that the protein–protein interactions that mediate dimerization did not survive the ionization process. However, dimeric FNR was also detected in the *m/z* spectrum (Fig. 2*A*), and in the deconvoluted spectrum (Fig. S1*A*), a broad low-intensity peak centered on 59,906 Da was observed that corresponds to dimeric FNR containing iron-sulfur clusters. There is a shoulder at the predicted mass for the [4Fe-4S] FNR dimer (59,794 Da), but the more intense peaks correspond to various adduct species, including likely single (+56 Da) and double (+112 Da) iron adducts. Optimization of experimental conditions for the transmission of dimeric species (2,750–5,000 *m/z*) provided sharper, better resolved dimer charge states (Fig. S1*C*). The deconvoluted spectrum of dimeric [4Fe-4S] FNR (Fig. 2*C*) contained a well-resolved peak centered on 59,796 Da, indicative of dimeric [4Fe-4S] FNR; around the dimer peak were a number of poorly resolved features, with the principal high-mass species caused by one covalently modified subunit within the dimer at +40 Da. No peaks for dimeric [2Fe-2S] or apo-FNR species were observed, consistent with them being monomeric in solution.

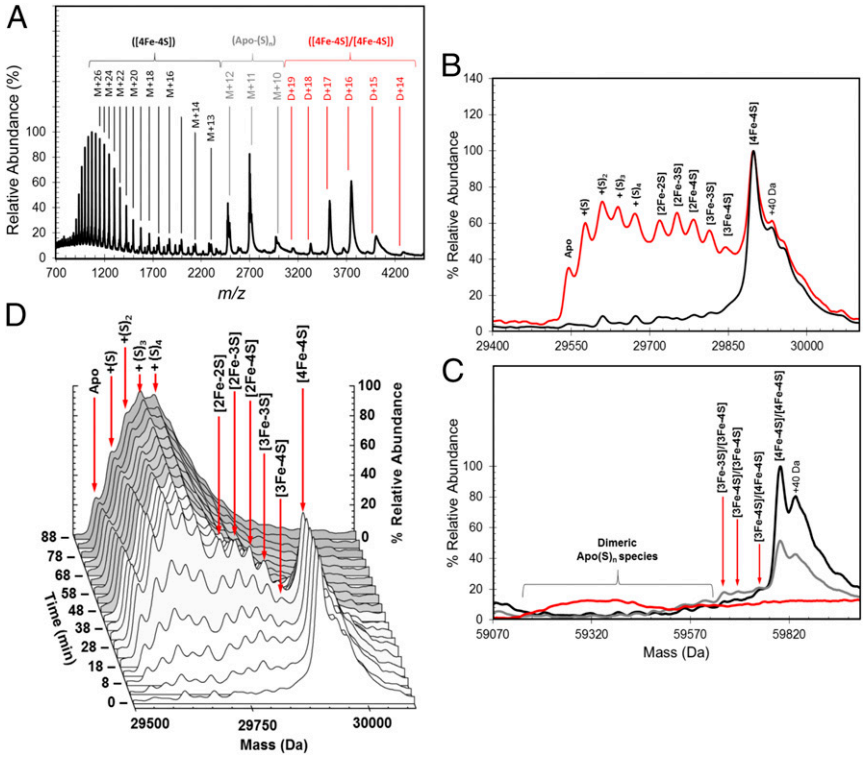

Fig. 2. ESI-MS of [4Fe-4S] FNR and the effect of exposure to O_2. (*A*) Full *m/z* spectrum for FNR. Charge states corresponding to monomeric [4Fe-4S] (black), persulfide adducts of apo (gray), and dimeric [4Fe-4S] (red) FNR species are shown. (*B*) Deconvoluted mass spectrum of [4Fe-4S] S24F FNR (black line) before and after exposure to dissolved atmospheric oxygen (18 min exposure; red line). This exposure results in the formation of a variety of protein-bound clusters, including [3Fe-4S], [3Fe-3S], and [2Fe-2S] forms. Persulfide adducts of [2Fe-2S] and apoprotein are also observed. (*C*) Deconvoluted spectrum of dimeric FNR showing the presence of the [4Fe-4S]/[4Fe-4S] form under anaerobic conditions and only low-intensity features caused by cluster conversion species after the addition of O_2 [20 (gray line) and 80 min (red line)]. The longer exposure time resulted in the loss of all cluster-containing dimer species, and the appearance of a broad, poorly resolved feature centered on 59,320 Da, approximating the mass of FNR containing multiple sulfane sulfurs (S^0_n, $n^{ave} \sim 8$). (*D*) 3D plot showing the formation and decay of all monomeric FNR species during the O_2 reaction time course. Spectra are representative of multiple repeat experiments.

ESI-MS Reveals Mechanism of O_2 Sensing. To study the mechanism of O_2 sensing by FNR, optimized ionization conditions for detection of the monomeric rather than dimeric form of [4Fe-4S] FNR were used, so that intermediate species could be clearly and unambiguously identified (Fig. 2*B*). The addition of O_2 (under pseudofirst-order reaction conditions where the $[O_2]$:[4Fe-4S] ratio was ~10) resulted in the formation of a complex series of overlapping peaks (Fig. 2*B*). These peaks can be subdivided into two distinct groups corresponding to protein-bound cluster fragments (29,700–29,850 Da) and sulfur adducts of apo-FNR (29,550–29,700 Da). The cluster-bound fragments include the [2Fe-2S] end product of the cluster conversion reaction (at 29,720 Da) along with species with masses that correspond to [2Fe-3S] (29,752 Da) and [2Fe-4S] (29,784 Da) forms, which most likely represent singly and doubly persulfide-coordinated [2Fe-2S] clusters, respectively, as recently shown by resonance Raman (16) (**3** and **4**). In addition, a peak corresponding to a [3Fe-4S] form that is a well-characterized intermediate of the cluster conversion process (13, 14) was observed at 29,843 Da (Table 1). Each of these species has been previously observed in solution using various spectroscopic methods. The spectra also contained a peak at 29,811 Da consistent with the presence of a [3Fe-3S] cluster form (Table 1), which may represent a previously undetected intermediate in the conversion process, in which one of two sulfides that are eventually lost from the original [4Fe-4S] cluster has been ejected.

To investigate further these intermediates of cluster conversion, a ^{34}S-substituted form of [4Fe-4S] FNR was generated (16) The deconvoluted spectrum contained a major peak at 29,905 Da, +8 Da relative to the predicted mass of natural abundance [4Fe-4S] FNR (Fig. 3*A*). The predicted increase in mass on substitution of all sulfides is +7.6 Da (calculated from natural isotope abundance). Exposure of the ^{34}S-labeled [4Fe-4S] FNR sample to O_2 resulted in cluster conversion as described above, except that the peaks corresponding to the cluster breakdown products were mass shifted as follows: [3Fe-4S] by +8 Da, [2Fe-2S] by +4 Da, [2Fe-3S] by +6 Da, and [2Fe-4S] by +8 Da (Fig. 3 *A* and *B*). The isotope substitution data also showed that the sulfur adducts of apo-FNR observed after reaction of [4Fe-4S] FNR with O_2 are derived from the cluster (Fig. 3*C*) and that oxygen adducts of FNR are not formed (Fig. S2). Overall, the isotope substitution data provide unambiguous confirmation of the assignments for the cluster conversion intermediates and products.

To investigate the kinetic behavior of these species, [4Fe-4S] FNR was combined with excess dissolved O_2 and continuously infused into the ESI source of the instrument. Fig. 2*D* shows the deconvoluted spectra obtained during the reaction time course over 120 min. Identical measurements of FNR that was not exposed to O_2 before infusion showed that the changes observed were entirely caused by O_2 exposure. At the earliest time points, a series of overlapping peaks identical in mass to those in Fig. 2*B* was observed. Peaks corresponding to the protein-bound cluster fragments (29,700–29,850 Da) increased in intensity, reaching a maximum ~15–30 min post-O_2 exposure. During this period, the [4Fe-4S] peak remained the most abundant species before

Table 1. Predicted and observed masses for cluster-bound forms of FNR

FNR species	Predicted mass (Da)*	Average observed mass (Da)†	ΔMass (Da)‡
Monomeric FNR			
$[4Fe\text{-}4S]^{2+}$	29,897	29,898	+1
$[3Fe\text{-}4S]^{1+}$	29,842	29,843	+1
$[3Fe\text{-}3S]^{3+}$	29,808	29,811	+3
$[3Fe\text{-}3S]^{1+}$	29,810	29,811	+1
$[2Fe\text{-}4S]^{2+}$	29,785	29,784	−1
$[2Fe\text{-}3S]^{2+}$	29,753	29,752	−1
$[2Fe\text{-}2S]^{2+}$	29,721	29,720	−1
Dimeric FNR			
$[4Fe\text{-}4S]^{2+}/[4Fe\text{-}4S]^{2+}$	59,794	59,796	+2
$[4Fe\text{-}4S]^{2+}/[3Fe\text{-}4S]^{1+}$	59,739	59,740	+1
$[3Fe\text{-}4S]^{1+}/[3Fe\text{-}4S]^{1+}$	59,684	59,685	+1
$[3Fe\text{-}3S]^{3+}/[3Fe\text{-}4S]^{1+}$	59,650	59,653	+3
$[3Fe\text{-}3S]^{1+}/[3Fe\text{-}4S]^{1+}$	59,652	59,653	+1

*The difference in predicted mass depending on the overall charge on the cluster is caused by charge compensation of cluster binding. A lower overall cluster charge would result in more protons remaining bound and consequently, a higher mass (26, 34).
†The average observed mass is derived from at least four independent experiments, with SD of ±1 Da.
‡The difference between the average observed and predicted masses.

decaying away along with the protein-bound cluster fragment peaks at later time points. In contrast, peaks corresponding to sulfur adducts of apo-FNR continued to rise to a maximum ∼30–50 min postexposure (Fig. 2*D*).

Abundances of the different cluster fragments and apoprotein species in Fig. 2*D* were plotted as a function of time. In MS experiments, abundances are reported relative to the most abundant species (arbitrarily set to 100%). For FNR experiments, the most abundant species over most of the time course was the [4Fe-4S] cluster, and therefore, these data fail to provide any information on the rate of [4Fe-4S] cluster decay. To enable global analysis to be performed, absorbance spectroscopy was, therefore, used to measure (at 406 nm) the decay of the cluster under conditions identical to those used for MS experiments. The absorbance data were converted to relative abundance (with the starting point set to 100%) for direct comparison with the MS data. Global analysis of multiple ($n = 4$) mass spectrometric kinetic datasets leads to the reaction scheme shown in Fig. 4*A*. This scheme was able to model the formation and/or decay of the peak intensities corresponding to the previously characterized [4Fe-4S], [3Fe-4S], [2Fe-2S], and apo-FNR species (Fig. 4*B*), indicating that the [3Fe-4S] cluster is the first intermediate formed (maximizing before 20 min) followed by [2Fe-2S] and apo-FNR. The temporal nature of [3Fe-3S], which maximized at ∼20 min (Fig. 4*C*), is consistent with an intermediate in the [4Fe-4S] to [2Fe-2S] cluster conversion pathway. However, both the [2Fe-4S] and [2Fe-3S] species (persulfide-coordinating forms of [2Fe-2S]) also reach a maximum at ∼20 min before the [2Fe-2S] cluster (∼30 min) (Fig. 4 *D* and *E*, respectively). The data show that [2Fe-3S] is not formed from [2Fe-2S] or the reverse; rather, [3Fe-3S] clusters can give rise to both [2Fe-3S] and [2Fe-2S] clusters, and therefore, this part of the reaction represents a branch point in an otherwise largely linear reaction mechanism. Similarly, the [2Fe-4S] cluster must form from [3Fe-4S] (and not [3Fe-3S]), and therefore, the formation of this species represents a second branch point (Fig. 4*A*).

The time dependence of intensity in the apoprotein region indicates that apo-FNR was converted to sulfane-containing species, apo$(S)_n$, with essentially full conversion at ∼80 min (Fig. 4*B*). Indeed, the global fit was dependent on this being part of the mechanistic scheme (Fig. 4*A*). Similarly, the [2Fe-3S] and [2Fe-4S] clusters, which both contain persulfides, give rise to apo$(S)_n$ species after the disassembly of their ligated [2Fe-2S] cluster as shown in Fig. 4*A*. An important feature of the data (both from MS and absorbance spectroscopy) is that the rate at which the apoprotein is formed from [2Fe-2S] in ammonium acetate buffer is greater than that previously reported for other buffer systems (13, 14). The poor stability of [2Fe-2S] species under these conditions means that they decay away in the MS spectrum rather than accumulating.

Overall, the model describes the behavior of the main [4Fe-4S], [3Fe-4S], and [2Fe-2S] cluster species, previously identified by spectroscopy, and the appearance of the [3Fe-3S], [2Fe-4S], [2Fe-3S], and apo-FNR species, all observed here simultaneously by MS (Fig. 4 *B*–*E*). We note that the model indicates that direct conversion of the [4Fe-4S] cluster to the [3Fe-3S] species does not occur. Thus, loss of a single iron seems to be an obligatory first step in the cluster conversion process, with loss of sulfide following that step.

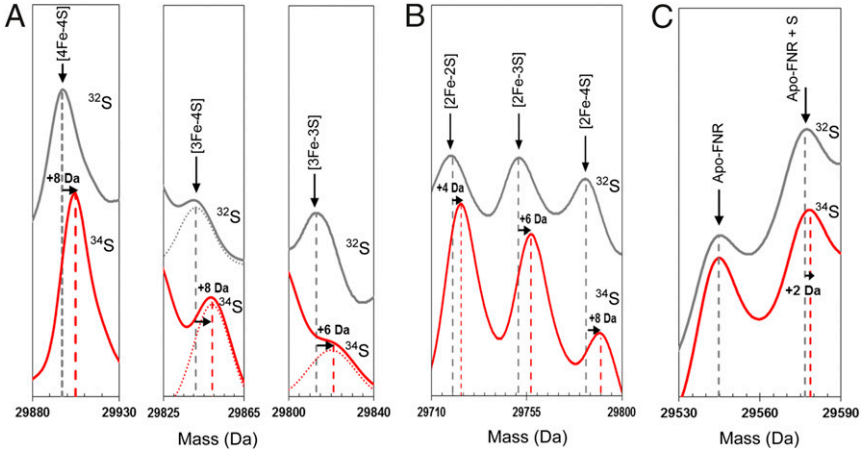

Fig. 3. Mass shifts observed for the FNR [4Fe-4S] cluster, conversion intermediates, and cluster products on ^{34}S substitution of cluster sulfides. (*A*) Deconvoluted mass spectra of natural abundance sulfur [4Fe-4S] S24F FNR and cluster conversion intermediates (black lines) and the equivalent ^{34}S-substituted forms (red lines) as indicated. Dotted lines represent Gaussian fits of the MS data. (*B*) The same as in *A* except that spectra represent cluster conversion products as indicated. (*C*) The same as in *A* except that spectra show the apo-FNR peak and the first persulfide adduct. Predicted mass shifts for the assigned species are indicated.

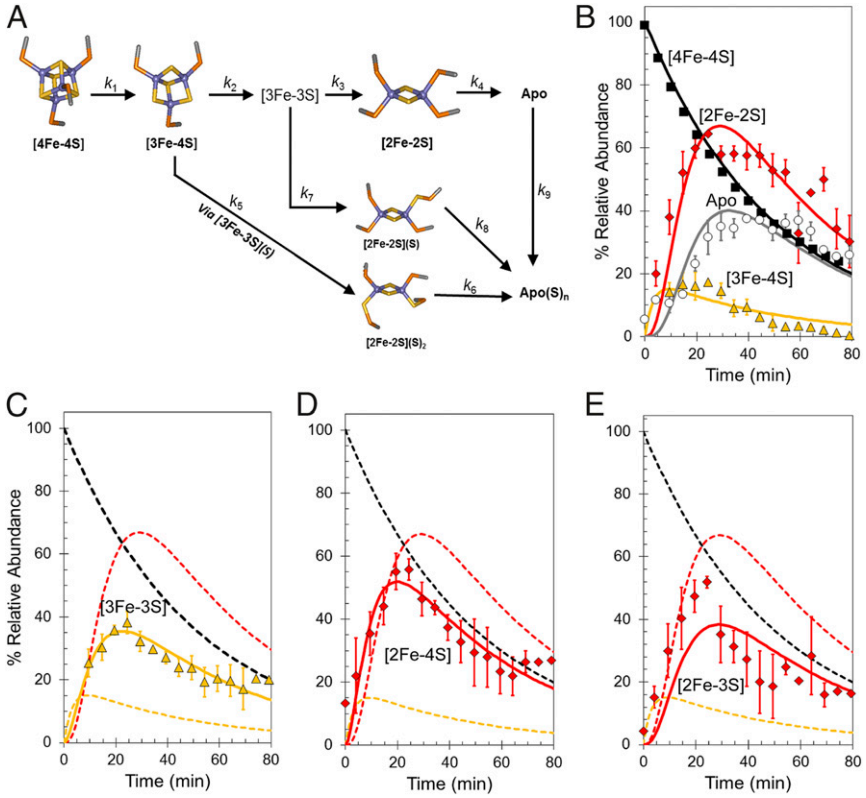

Fig. 4. Mechanism of [4Fe-4S] cluster conversion. (*A*) Reaction scheme used to simulate the kinetic dependence native MS data. (*B*) Plots of relative abundances of [4Fe-4S] cluster ($A_{406\ nm}$; black squares), [3Fe-4S] (yellow triangles), [2Fe-2S] cluster (red diamonds), and apo (white circles) species as a function of time after exposure to excess O_2. Global fitting to the experimental data using the reaction scheme depicted in *A* is shown as solid lines. (*C*–*E*) Plots of relative abundances of the [3Fe-3S] cluster (yellow triangles in *C*), the [2Fe-4S] cluster (red diamonds in *D*), and the [2Fe-3S] cluster (red diamonds in *E*). Global fits to the experimental data are shown as solid lines. Dashed lines in *C*–*E* show the responses of the [4Fe-4S], [3Fe-4S], and [2Fe-2S] clusters for easy comparison. Error bars show SEs for average MS datasets ($n = 4$). The global fitting model was initiated with 100% relative abundance of [4Fe-4S] clusters.

Table 2 shows the observed rate constants required to describe the reaction scheme depicted in Fig. 4*A*. The first reaction, corresponding to the conversion of the [4Fe-4S] cluster into the [3Fe-4S] cluster, has an observed rate constant (k_{obs1}) of 0.02 min^{-1} (0.003 s^{-1}), implying that it is rate limiting as previously observed (13, 14). Division of k_{obs1} by the O_2 concentration (122 μM) used here provides an estimate of the apparent second-order rate constant, $k = 25\ M^{-1}\ s^{-1}$. This value is lower than the previously reported value of 80 $M^{-1}\ s^{-1}$ for S24F FNR (28). It is known that the [4Fe-4S] to [2Fe-2S] cluster conversion is influenced by the nature of the buffer environment, in this case ammonium acetate.

Kinetics of Persulfide Adduct Formation Determined by LC-MS. LC-MS, in which protein samples are in denaturing solvent, can be used to follow the formation of sulfane adducts during Fe-S cluster reactions, because these adducts are covalent species that survive protein unfolding (29). LC-MS was applied to samples of FNR equivalent to those used for native MS experiments. The reaction was quenched at specific time points to halt the reaction and inhibit any subsequent sulfur exchange, so that the time evolution of sulfane adducts could be correlated with the native MS data and used to monitor cluster sulfide oxidation. In the absence of O_2, the major peak at 29,547 Da corresponded to apo-FNR without sulfur adducts (Fig. 5). Shoulder peaks at +32, +64, and +96 Da are caused by the addition of one, two, and three sulfane sulfur atoms, respectively (29).

The addition of O_2 resulted in a 2-Da shift in the apo-FNR to 29,545 Da, consistent with the presence of a single disulfide bond. In addition, there was an increased abundance of peaks corresponding to the sulfane adducts as previously observed (16) (Fig. 5). As can be seen from Fig. 5*B*, the single or double sulfane adducts of FNR become the major species with increasing time. The time dependence of their appearance shows that sulfide oxidation occurs simultaneously with cluster conversion. From the native MS experiments above, it was suggested that the [2Fe-3S] and [2Fe-4S] species give rise to the single and double sulfane forms of apo-FNR, respectively, after the disassembly of the persulfide-ligated [2Fe-2S] cluster. The temporal appearance of the single and double sulfane adducts, maximizing at ∼30–40 min, supports this hypothesis (Fig. S3).

Table 2. Observed rate constants used to fit experimental data shown in Fig. 4 *B*–*E* to the cluster disassembly model shown in Fig. 4*A*

Reaction step	Observed rate constant (min^{-1})*	Reaction
k_1	$0.020 \pm 5 \times 10^{-5}$	[4Fe-4S] → [3Fe-4S]
k_2	0.123 ± 0.002	[3Fe-4S] → [3Fe-3S]
k_3	0.072 ± 0.001	[3Fe-3S] → [2Fe-2S]
k_4	0.200 ± 0.003	[2Fe-2S] → apo
k_5	0.200 ± 0.003	[3Fe-4S] → [2Fe-4S]
k_6	0.145 ± 0.003	[2Fe-4S] → apo$(S^0)_n$
k_7	0.040 ± 0.001	[3Fe-3S] → [2Fe-3S]
k_8	0.210 ± 0.006	[2Fe-3S] → apo$(S^0)_n$
k_9	0.330 ± 0.008	apo → apo$(S^0)_n$

*SEs are indicated.

The apo(S)$_n$ species detected by LC-MS result from not only the presence of apo(S)$_n$ species in solution but also, denaturation of cluster-bound sulfane adducts present at the point of quenching, and these adducts cannot be distinguished in the LC-MS experiment. However, because the [2Fe-2S] forms are not stable in the ammonium acetate buffer of the native MS experiment, the kinetic profiles of formation of apo(S)$_n$ species in the LC-MS are similar to those in the native MS experiment, and the LC-MS data could be readily modeled by extending the initial mechanistic model (Fig. 5*C*) to reflect the proposed fate of the [2Fe-2S] clusters (Fig. S3). An important feature of the extended model is that apo(S)$_{n\ =\ 1–4}$ species are in equilibrium with each other, implying that sulfide is readily mobilized from one species to another, presumably via disulfide exchange. The extended model, initiated with [4Fe-4S] FNR at 100% relative abundance, describes the appearance of the apo(S)$_{n\ =\ 1–3}$ adducts detected via LC-MS and importantly, was also able to model the formation of apo(S)$_n$ species detected by native MS (Fig. 5*D*). The observed rate constants obtained from the experimental data fits (Fig. 5*D* and Fig. S3) are given in Table 3.

Cluster Reactivity of Dimeric [4Fe-4S] FNR. Under conditions where the ionization of dimeric FNR was optimized, addition of O_2 resulted in three low-intensity peaks that increased in intensity with time, reaching a maximum at ~15 min, before decaying away along with all cluster-bound forms (Fig. 2*B*). These peaks correspond to dimeric FNR containing a [3Fe-4S] and [4Fe-4S] cluster (59,740 Da), two [3Fe-4S] clusters (59,685 Da), and a [3Fe-3S] and [3Fe-4S] cluster (59,653 Da) (Fig. S4). The low intensity of these peaks is consistent with cluster conversion initiating the dimer to monomer transition, such that only the [4Fe-4S] cluster can maintain a significant population of dimeric FNR. The equilibrium between monomer and dimer is apparently shifted toward monomer forms when [3Fe-4S] or [3Fe-3S] clusters are bound. With increasing time, a large, broad, and poorly resolved feature appeared. The average mass of this feature was ~59,348 Da, and it is most likely caused by disulfide-linked dimeric FNR, with an average of eight additional sulfur atoms.

Discussion

Here, we have used mass spectrometry to investigate the O_2-mediated conversion of the [4Fe-4S] cluster of FNR to a [2Fe-2S] form, which causes dissociation of the FNR dimer into monomers and loss of high-affinity DNA binding (7–14). The S24F variant of FNR was used for this study, because previous studies showed that it reacts via the same two-step mechanism (**1** and **2**) as WT FNR but at a slower rate (28), enabling real-time mass spectrometry measurements. Thus, it is reasonable to conclude that the intermediates uncovered in this work also occur in WT FNR. The data presented here provide remarkable mechanistic detail of the conversion process.

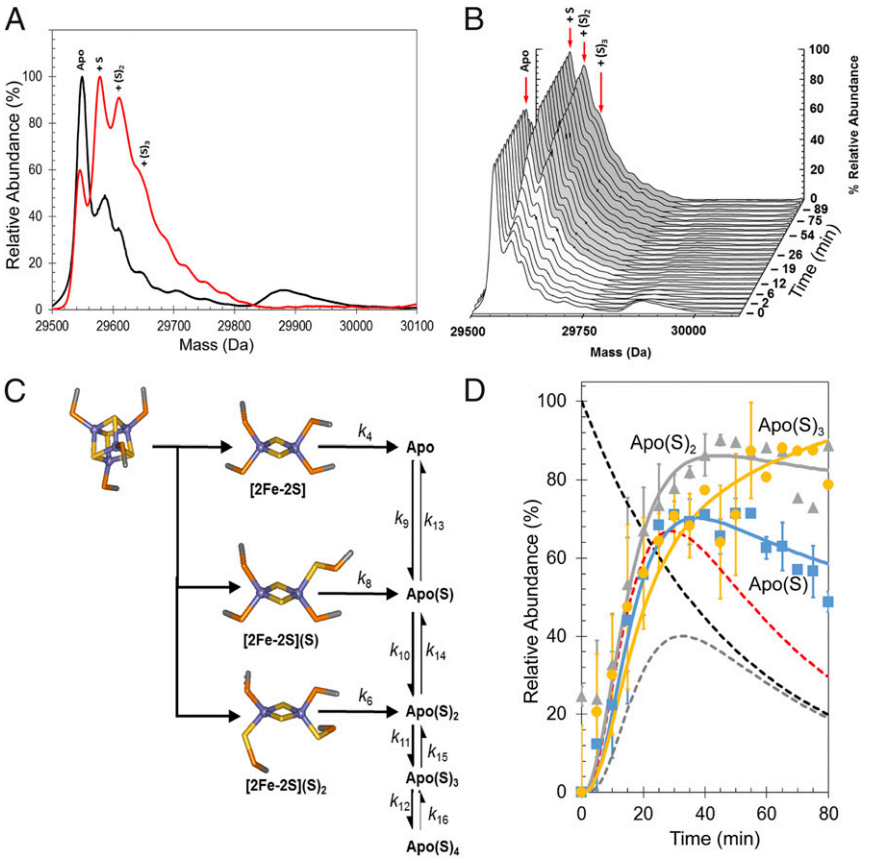

Fig. 5. Tracking sulfide oxidation by LC-MS and native MS. (*A*) Deconvoluted LC-MS spectra before (black line) and after (red line) exposure to excess O_2 reveal the formation of persulfide adducts. The broad feature at 29,900 Da in the anaerobic spectrum corresponds to poorly resolved cluster fragments. (*B*) Survey plot showing the formation of persulfide adducts during the reaction time course. (*C*) Abbreviated reaction scheme based on that in Fig. 3*A* used to simulate the kinetic behavior of FNR persulfide species. (*D*) Plots of relative abundances of the apo-S (blue squares), apo-SS (gray triangles), and apo-SSS (yellow circles) species detected in native MS experiments. Global fitting to the experimental data using the reaction scheme depicted in Fig. 4*C* is shown as solid lines. Dashed lines show the responses of the [4Fe-4S] (black), [2Fe-2S] (red), and apo (gray) species for comparison. Error bars show SEs for average MS datasets (n = 4). The global fitting model was initiated with 100% relative abundance of [4Fe-4S] clusters.

Table 3. Observed rate constants used to fit experimental data shown in Fig. 5*D* and Fig. S3 to the apo(S)$_n$ model shown in Fig. 5*C*

Reaction step	Observed rate constant (min^{-1})*	Reaction
$k_{1–8}$	Table 2	Cluster disassembly model
k_9	0.900 ± 0.02	apo → apo(S)
k_{13}	0.050 ± 0.004	apo ← apo(S)
k_{10}	1.000 ± 0.01	apo(S) → apo(S)$_2$
k_{14}	0.400 ± 0.006	apo(S) ← apo(S)$_2$
k_{11}	1.000 ± 0.009	apo(S)$_2$ → apo(S)$_3$
k_{15}	0.900 ± 0.01	apo(S)$_2$ ← apo(S)$_3$
k_{12}	0.980 ± 0.01	apo(S)$_3$ → apo(S)$_4$
k_{16}	0.034 ± 6 × 10^{-4}	apo(S)$_3$ ← apo(S)$_4$

*SEs are indicated.

ESI-MS experiments, including cluster-specific ^{34}S isotopic substitution, and global analysis are consistent with previous spectroscopic studies showing that the first step of the reaction is the loss of Fe^{2+} from the $[4Fe\text{-}4S]^{2+}$ cluster to form a $[3Fe\text{-}4S]^{1+}$ cluster intermediate (13, 14, 30). This process is assumed to occur via oxidation of the cluster to an oxidized state, $[4Fe\text{-}4S]^{3+}$, that immediately ejects an Fe^{2+} ion, forming the $[3Fe\text{-}4S]^{1+}$ species (13, 30). After it is formed, the $[3Fe\text{-}4S]^{1+}$ cluster is only transiently stable, ejecting an Fe^{3+} ion together with two sulfide ions (S^{2-}) to generate the $[2Fe\text{-}2S]^{2+}$ cluster form of FNR. Little is known about the rearrangement of the $[3Fe\text{-}4S]^{1+}$ cluster to the $[2Fe\text{-}2S]^{2+}$ form. The ESI-MS data reported here provide key insights into this. The detection of a [3Fe-3S] cluster that kinetic modeling shows is a cluster conversion intermediate results from the loss of one sulfide ion from the $[3Fe\text{-}4S]^{1+}$ cluster, implying that the product is a $[3Fe\text{-}3S]^{3+}$ species. An inorganic model $[3Fe\text{-}3S]^{3+}$ cluster has recently been described for the first time, in which all iron and sulfide ions are in the same molecular plane forming a hexagonal arrangement (31). Previous studies of the [3Fe-4S] cluster of FdI ferredoxin from *Pyrococcus furiosus* by nondenaturing ESI Fourier transform ion cyclotron resonance MS revealed the presence of a $[3Fe\text{-}3S]^{3+}$ cluster form along with other cluster breakdown species (26). In that case, the instability of the cluster was caused by ionization (the initial [3Fe-4S] cluster was stable in negative ion mode), but it provides clear independent evidence for the existence of a protein-bound [3Fe-3S] cluster. In the case of FNR, the charge state of the [3Fe-3S] cluster is not established. Assumption of a 3+ overall charge resulted in a reproducible difference between observed and predicted masses (Table 1). However, if 1+ charge is assumed, a very close match between observed and predicted masses was obtained. The same is true for the dimeric FNR species with [3Fe-3S] clusters bound. An overall charge of +1 on the cluster may arise from oxidation of the first sulfide released from the $[3Fe\text{-}4S]^{1+}$ intermediate (that is, by release of sulfane).

A key feature of our kinetic model of the [3Fe-4S] to [2Fe-2S] conversion process is that the $[3Fe\text{-}4S]^{1+}$ intermediate rapidly loses either a sulfide ion or a sulfane atom to form the $[3Fe\text{-}3S]^{1+}$ or $[3Fe\text{-}3S]^{3+}$ cluster, which undergoes additional reaction relatively slowly. Hence, conversion of the [3Fe-3S] intermediate is the rate-limiting step of this process. The observed rate constant (k_3 in Fig. 4 and Table 2) of 0.072 min^{-1} (1.2 × 10^{-3} s^{-1}) is comparable with that previously reported for the [3Fe-4S] to [2Fe-2S] conversion for both the S24F variant (5 × 10^{-4} s^{-1}) and WT FNR (1.7 × 10^{-3} s^{-1}) (28). This similarity suggests that the intermediate cluster species previously detected by EPR may actually be a [3Fe-3S] cluster rather than a [3Fe-4S] species as previously concluded, or it could be a mixture of the two. Analysis of the magnetic properties of the model $[3Fe\text{-}3S]^{3+}$ cluster species revealed a paramagnetic S = 1/2 ground state (31), which gives rise to an X-band EPR spectrum that is similar to those of $[3Fe\text{-}4S]^{1+}$ cluster proteins (31, 32) as well as that recorded for the FNR cluster conversion intermediate in both WT and S24F FNR (14, 28). This similarity could indicate that $[3Fe\text{-}3S]^{3+}$ is formed on FNR, but we note that $[3Fe\text{-}3S]^{1+}$ would also be paramagnetic, although the EPR properties of such a cluster are unknown.

Assuming that the hexagonal planar arrangement of the three Fe^{3+} and sulfide ions in the model [3Fe-3S] cluster is also a feature of the FNR [3Fe-3S] species (Fig. S5), this arrangement suggests how the cuboid [4Fe-4S] cluster may rearrange to form the planar [2Fe-2S] rhomb, the process that drives the key structural rearrangement of FNR leading to monomerization and loss of DNA binding. Support for this proposal comes from the dimeric FNR MS data, which strikingly shows that, although the [4Fe-4S]/[4Fe-4S] FNR dimer was readily detected, only very minor amounts of [3Fe-4S]/[4Fe-4S], [3Fe-4S]/[3Fe-4S], and [3Fe-3S]/[3Fe-4S] species were observed. We note that these species could alternatively correspond to different combinations of clusters (e.g., the [3Fe-4S]/[3Fe-4S] species could also be a [2Fe-4S]/[4Fe-4S] species), but the fact that they are minor compared with the [4Fe-4S]/[4Fe-4S] form remains. This ambiguity emphasizes the importance of the monomer region for definitive identification of cluster forms. If the [3Fe-3S] cluster formed is planar, then the accompanying structural rearrangement, involving conversion from a tetrahedral to a planar arrangement of coordinating Cys residues, would be expected to disrupt the dimer as observed in the MS data. Furthermore, the relatively rapid conversion of [3Fe-4S] to [3Fe-3S] would account for the failure of [3Fe-4S] species to accumulate in the MS spectra of the FNR dimer region. The temporal behavior of the low-intensity FNR dimer cluster conversion species matches well that observed for the monomeric FNR [3Fe-4S] and [3Fe-3S] intermediates, consistent with dissociation of dimeric FNR species into monomer forms.

Loss of sulfide during conversion of [3Fe-4S] to [3Fe-3S] might be compensated for through reengagement of the Cys residue that detaches when the initial Fe^{2+} is lost (Fig. S5). We note that a dimeric form of AfFNR, containing a partly degraded cluster (possibly a 3Fe cluster), displays a disorganized cluster binding loop (residues 20–29) after the loss of iron(s) (6). Thus, the data strongly indicate that, as soon as an Fe^{2+} ion is lost from one $[4Fe\text{-}4S]^{2+}$ cluster (on one of the subunits of the dimer), the stability of the dimer is reduced and that the monomer–dimer equilibrium becomes heavily favored in the direction of the monomer.

Recently, it was shown that cluster sulfide is oxidized to sulfane, with incorporation into Cys residues as persulfides that coordinate the [2Fe-2S] form of FNR (16). Cys persulfides, as a stored form of sulfur, allow the original cluster to be repaired on supply of electrons and Fe^{2+} as shown in vitro (16). The formation of persulfides raises questions about when sulfide oxidation occurs in relation to cluster conversion: simultaneously with the conversion process or subsequent to it in an additional reaction. The MS data resolve this question. Analysis of the kinetic data shows that sulfide oxidation occurs at the same time as formation of the [2Fe-2S] cluster, leading to [2Fe-2S] and singly and doubly persulfide-coordinated species forming simultaneously. The [3Fe-3S] intermediate identified here undergoes loss of Fe^{3+} and loss/oxidation of sulfide to [2Fe-2S](S) and [2Fe-2S], representing a branch point of the mechanism. Clearly, [2Fe-2S](S)$_2$ cannot be formed directly from [3Fe-3S] but instead, must form from [3Fe-4S], and therefore, it represents a second branch point. By analogy with the above, this reaction is likely to occur via a [3Fe-3S](S) intermediate, where the sulfide is oxidized to sulfane and released from the cluster but retained on a Cys as a persulfide. This species cannot be distinguished from the [3Fe-4S] intermediate in the MS spectrum. This ambiguity may be the reason why the global fit to the [3Fe-4S] species kinetic profile is not as good as for the other cluster intermediates; the data actually represent a combination of [3Fe-4S] and [3Fe-3S](S) species.

A fit of the data based on a revised model in which this additional step is included (Fig. S6) is consistent with this proposal. The simultaneous nature of cluster conversion and sulfide oxidation was confirmed by LC-MS experiments carried out under identical conditions to the native MS experiments.

The formations of a Cys persulfide by oxidative coupling of a sulfide from the trisulfide face of the [3Fe-4S] cluster or the putative hexagonal ring of a [3Fe-3S] cluster with a nearby free cysteine are both plausible paths. Presumably, electrons from sulfide oxidation reduce O_2 to either H_2O_2 or water, accounting for the observed stoichiometry for the cluster conversion reaction of ∼1.5 O_2 consumed per cluster (30). Cluster iron oxidation yields only one electron. The other electrons must be derived from sulfide oxidation, resulting, overall, in a mixture of superoxide (where no sulfide oxidation occurs), hydrogen peroxide, and water (14, 16).

In conclusion, the ESI-MS results, with the benefit of previously published spectroscopic and kinetic analyses, provide insight into the mechanism by which O_2 sensing occurs in FNR. A global kinetic analysis of the starting, intermediate, and product species yields unsuspected aspects of the mechanistic model. Not only has a previously unrecognized [3Fe-3S] cluster intermediate species been identified, but the nature of sulfide oxidation to generate persulfide species has also been resolved. This work further shows the feasibility of time-resolved ESI-MS for the study of iron-sulfur clusters and their reactions within a protein framework, with potential broad application to studies of other systems involving interactions/reactions of protein cofactors with small molecules.

Materials and Methods

Protein Purification. A plasmid for the expression of C-terminal $(His)_6$-tagged *E. coli* S24F FNR, in which the mutant *fnr* gene was ligated into pGS21a plasmid (Genscript) at NdeI and HindIII sites, was purchased (Genscript) (Fig. S7). Protein was overproduced in *E.coli* (BL21 λDE3 Star) cultures as previously described (28), except that 0.4 mM isopropyl β-D-thiogalactoside was used to induce protein expression. For minimal media growth preparations, cultures were grown in M9 minimal media as previously described (33). Cells were harvested by centrifugation, lysed on ice by sonication in buffer A (25 mM Hepes, 2.5 mM $CaCl_2$, 100 mM NaCl, 100 mM $NaNO_3$, pH 7.5) with 500 mM KCl, and centrifuged at 40,000 × *g* for 45 min at 4 °C. Inside an anaerobic cabinet (O_2 < 2 ppm; Belle Technology), the cleared cell lysate was loaded onto a HiTrap (GE Healthcare) Ni^{2+}-chelating column (2 × 5 mL) with 14% (vol/vol) buffer B (buffer A with 500 mM KCl, 500 mM imidazole, pH 7.5) and washed until $A_{280\ nm} \leq 0.1$. Bound proteins were eluted using a linear gradient (10 mL) from 14 to 100% buffer B. Fractions (1 mL) containing FNR were pooled and immediately desalted into buffer C (buffer A with 2 mM DTT, pH 7.5) via a HiTrap desalting column (4 × 5 mL). As isolated, samples were ≤50% replete with cluster. To increase cluster loading, [4Fe-4S] clusters were inserted via an NifS catalyzed in vitro reconstitution reaction, from which the protein was reisolated using a HiTrap Heparin column as previously described (33). Bound protein was eluted using buffer A with 500 mM KCl, pH 7.5. Residual apo-S24F (∼30 kDa) was separated from holo-S24F (∼60 kDa) via gel filtration with a calibrated Sephacryl S100HR column previously equilibrated with buffer D (50 mM Tris, 300 mM KCl, 2 mM DTT, pH 8.0). Dimeric holo-S24F–containing fractions were pooled and frozen as described previously (14). ^{34}S-substituted [4Fe-4S] S24F FNR was prepared using ^{34}S-labeled cysteine in a reconstitution reaction as previously described (16).

Mass spectrometry. For native ESI-MS, an aliquot of S24F FNR was exchanged into buffer E (250 mM ammonium acetate, pH 6.7) using Zeba spin (Thermo Scientific) or midi-PD10 (GE Healthcare) desalting columns; the volume of the eluent was increased to 2 mL, and the concentration of [4Fe-4S] S24F FNR was determined via absorbance at 406 nm (see below). An aliquot of the sample was combined with an aliquot (1.6 mL) of buffer E containing dissolved atmospheric O_2 (168 μM O_2; final concentration) in an anaerobic cuvette to give ∼14 μM [4Fe-4S] S24F FNR. Buffer E lacking dissolved O_2 was used for control experiments. The sample was immediately loaded into a 1-mL gas-tight syringe (Hamilton) and infused directly using a syringe pump (0.3 mL/h) into the ESI source of a Bruker micrOTOF-QIII mass spectrometer (Bruker Daltonics) operating in the positive ion mode. The ESI-TOF was calibrated using ESI-L Low Concentration Tuning Mix (Agilent Technologies). Before the introduction of sample, the gas-tight syringe (Hamilton) and associated PEEK tubing (Upchurch Scientific) were flushed with 5 mL anaerobic buffer E. The oxygen permeability of PEEK tubing is 14 mL/250 cm^2 (1 atm/25 °C) over 24 h (Upchurch Scientific). MS data were acquired over the *m/z* range of 700–3,500 continuously for 120 min, with acquisition controlled using Bruker oTOF Control software and parameters as follows: dry gas flow of 4 L/min, nebulizer gas pressure of 0.8 Bar, dry gas at 180 °C, capillary voltage of 4,500 V, offset of 500 V, ion energy of 5 eV, collision radio frequency of 200 Vpp, and collision cell energy of 10 eV. Optimization of experimental conditions for the transmission of dimeric species (2,500–5,000 *m/z*) was achieved by increasing the equivalent of the cone voltage (in-source collision-induced dissociation of 75 eV), reducing the collision cell energy (4 eV), and increasing the collision RF (1,500 Vpp) (34).

For LC-MS, an aliquot of S24F FNR was exchanged into buffer E (120 μL; ∼252 μM [4Fe-4S]) using a Zeba spin column, and the volume of the eluent increased to 500 μL. For O_2 reactivity measurements, the sample was combined with an aliquot (1.6 mL) of oxygenated buffer E (∼14 μM [4Fe-4S], 168 μM O_2; final concentration) in an anaerobic cuvette and allowed to react. Samples (50 μL) were removed at varying time points and diluted to ∼1.5 μM (final concentration) with an aliquot (406 μL) of quenching solution [an aqueous mixture of 0.8 mM EDTA, 0.7% (vol/vol) formic acid, 2% (vol/vol) acetonitrile]. For experiments probing the reversibility of adduct formation before and after reaction with O_2, samples were treated with 20 mM DTT. Samples were sealed, removed from the anaerobic cabinet, and injected (1 μL) onto a ProSwift reversed phase RP-1S column (4.6 × 50 mm; Thermo Scientific) at 25 °C using an UltiMate 3000 HPLC system (Dionex).

Gradient elution was performed at a flow rate of 0.2 mL/min using a linear gradient (15 min) from 2 to 100% (vol/vol) acetonitrile and 0.1% (vol/vol) formic acid. The eluent was continuously infused into a Bruker micrOTOF-QIII mass spectrometer running Hystar (Bruker Daltonics) using positive mode ESI. The mass spectrometer was calibrated with ESI-L tuning mix (Agilent Technologies). MS acquisition parameters were as follows: dry gas flow of 8 L/min, nebulizer gas pressure of 1.8 Bar, dry gas at 240 °C, capillary voltage of 4,500 V, offset of 500 V, and collision RF of 650 Vpp.

Processing and analysis of MS experimental data were carried out using Compass DataAnalysis, version 4.1 (Bruker Daltonik). Neutral mass spectra were generated using the ESI Compass, version 1.3 Maximum Entropy deconvolution algorithm over a mass range of 29,000–31,000 Da for the monomer and 59,000–60,500 Da for the dimer. For kinetic modeling, to clearly resolve overlapping peaks, multiple Gaussian functions were fitted to the experimental data using a least squares regression function in Origin 8 (Microcal) (34). Exact masses are reported from peak centroids representing the isotope average neutral mass. For apoproteins, these masses are derived from *m/z* spectra, for which peaks correspond to $[M + nH]^{n+}/n$. For cluster-containing proteins, where the cluster contributes charge, peaks correspond to $[M + FeS^{x+} + (n - x)H]^{n+}/n$, where *M* is the molecular mass of the protein, FeS is the mass of the iron-sulfur cluster of *x*+ charge, *H* is the mass of the proton, and *n* is the total charge. In the expression, the *x*+ charge of the cluster offsets the number of protons required to achieve the observed charge state (*n*+) (26). Predicted masses are given as the isotope average of the neutral protein or protein complex in which cofactor binding is expected to be charge compensated (35). For time-resolved MS intensity data, kinetic schemes were modeled using Dynafit 4 (BioKin Ltd) (36).

Other Analytical Techniques. Protein concentrations were determined using the method of Bradford (Bio-Rad), with BSA as the standard and a previously determined correction factor of 0.83 (30). The iron and sulfide content of the protein was determined as described previously (15, 37), and the $[4Fe\text{-}4S]^{2+}$ cluster concentrations were determined using an $\varepsilon_{406\ nm}$ of 16.22 (±0.14) $mM^{-1}\ cm^{-1}$ (13, 28). An Oxygraph+ (Hansatech Instruments) was used to determine the dissolved oxygen content of buffer E (244 ± 3 μM). Absorption and CD measurements were made using a Jasco V550 UV-visible spectrophotometer and a Jasco J-810 spectropolarimeter, respectively. Kinetic data at $A_{406\ nm}$ were recorded via a fiber optic link as previously described (14).

ACKNOWLEDGMENTS. We thank the University of East Anglia for funding the purchase of the electrospray ionization mass spectrometer instrument. This work was supported by Biotechnology and Biological Sciences Research Council Grant BB/L007673/1 (to J.C.C., A.J.T., and N.E.L.B.).

1. Unden G, Bongaerts J (1997) Alternative respiratory pathways of *Escherichia coli*: Energetics and transcriptional regulation in response to electron acceptors. *Biochim Biophys Acta* 1320:217–234.
2. Unden G, Guest JR (1985) Isolation and characterization of the Fnr protein, the transcriptional regulator of anaerobic electron transport in Escherichia coli. *Eur J Biochem* 146:193–199.
3. Kiley PJ, Reznikoff WS (1991) Fnr mutants that activate gene expression in the presence of oxygen. *J Bacteriol* 173:16–22.
4. Guest JR (1995) The Leeuwenhoek Lecture, 1995. Adaptation to life without oxygen. *Philos Trans R Soc Lond B Biol Sci* 350:189–202.
5. Guest JR, Russell GC (1992) Complexes and complexities of the citric acid cycle in Escherichia coli. *Curr Top Cell Regul* 33:231–247.
6. Volbeda A, Darnault C, Renoux O, Nicolet Y, Fontecilla-Camps JC (2015) The crystal structure of the global anaerobic transcriptional regulator FNR explains its extremely fine-tuned monomer-dimer equilibrium. *Sci Adv* 1:e1501086.
7. Green J, Sharrocks AD, Green B, Geisow M, Guest JR (1993) Properties of FNR proteins substituted at each of the five cysteine residues. *Mol Microbiol* 8:61–68.
8. Khoroshilova N, Popescu C, Münck E, Beinert H, Kiley PJ (1997) Iron-sulfur cluster disassembly in the FNR protein of *Escherichia coli* by O_2: [4Fe-4S] to [2Fe-2S] conversion with loss of biological activity. *Proc Natl Acad Sci USA* 94:6087–6092.
9. Kiley PJ, Beinert H (1998) Oxygen sensing by the global regulator, FNR: The role of the iron-sulfur cluster. *FEMS Microbiol Rev* 22:341–352.
10. Khoroshilova N, Beinert H, Kiley PJ (1995) Association of a polynuclear iron-sulfur center with a mutant FNR protein enhances DNA binding. *Proc Natl Acad Sci USA* 92:2499–2503.
11. Lazazzera BA, Bates DM, Kiley PJ (1993) The activity of the *Escherichia coli* transcription factor FNR is regulated by a change in oligomeric state. *Genes Dev* 7: 1993–2005.
12. Lazazzera BA, Beinert H, Khoroshilova N, Kennedy MC, Kiley PJ (1996) DNA binding and dimerization of the Fe-S-containing FNR protein from *Escherichia coli* are regulated by oxygen. *J Biol Chem* 271:2762–2768.
13. Crack JC, et al. (2008) Influence of the environment on the $[4Fe\text{-}4S]^{2+}$ to $[2Fe\text{-}2S]^{2+}$ cluster switch in the transcriptional regulator FNR. *J Am Chem Soc* 130:1749–1758.
14. Crack JC, Green J, Cheesman MR, Le Brun NE, Thomson AJ (2007) Superoxide-mediated amplification of the oxygen-induced switch from [4Fe-4S] to [2Fe-2S] clusters in the transcriptional regulator FNR. *Proc Natl Acad Sci USA* 104:2092–2097.
15. Crack JC, Green J, Le Brun NE, Thomson AJ (2006) Detection of sulfide release from the oxygen-sensing [4Fe-4S] cluster of FNR. *J Biol Chem* 281:18909–18913.
16. Zhang B, et al. (2012) Reversible cycling between cysteine persulfide-ligated [2Fe-2S] and cysteine-ligated [4Fe-4S] clusters in the FNR regulatory protein. *Proc Natl Acad Sci USA* 109:15734–15739.
17. Nicolet Y, Rohac R, Martin L, Fontecilla-Camps JC (2013) X-ray snapshots of possible intermediates in the time course of synthesis and degradation of protein-bound Fe_4S_4 clusters. *Proc Natl Acad Sci USA* 110:7188–7192.
18. Banerjee S, Mazumdar S (2012) Electrospray ionization mass spectrometry: A technique to access the information beyond the molecular weight of the analyte. *Int J Anal Chem* 2012:282574.
19. Morgner N, Robinson CV (2012) Linking structural change with functional regulation-insights from mass spectrometry. *Curr Opin Struct Biol* 22:44–51.
20. Hopper JT, Robinson CV (2014) Mass spectrometry quantifies protein interactions–from molecular chaperones to membrane porins. *Angew Chem Int Ed Engl* 53: 14002–14015.
21. Housden NG, et al. (2013) Intrinsically disordered protein threads through the bacterial outer-membrane porin OmpF. *Science* 340:1570–1574.
22. Breuker K, McLafferty FW (2008) Stepwise evolution of protein native structure with electrospray into the gas phase, $10^{(-12)}$ to $10^{(2)}$ s. *Proc Natl Acad Sci USA* 105: 18145–18152.
23. Kaltashov IA, Zhang M, Eyles SJ, Abzalimov RR (2006) Investigation of structure, dynamics and function of metalloproteins with electrospray ionization mass spectrometry. *Anal Bioanal Chem* 386:472–481.
24. Sutherland DE, Willans MJ, Stillman MJ (2012) Single domain metallothioneins: Supermetalation of human MT 1a. *J Am Chem Soc* 134:3290–3299.
25. Kondrat FD, Kowald GR, Scarff CA, Scrivens JH, Blindauer CA (2013) Resolution of a paradox by native mass spectrometry: Facile occupation of all four metal binding sites in the dimeric zinc sensor SmtB. *Chem Commun (Camb)* 49:813–815.
26. Johnson KA, Verhagen MFJM, Brereton PS, Adams MWW, Amster IJ (2000) Probing the stoichiometry and oxidation states of metal centers in iron-sulfur proteins using electrospray FTICR mass spectrometry. *Anal Chem* 72:1410–1418.
27. Crack JC, et al. (2015) NsrR from Streptomyces coelicolor is a nitric oxide-sensing [4Fe-4S] cluster protein with a specialized regulatory function. *J Biol Chem* 290:12689–12704.
28. Jervis AJ, et al. (2009) The O_2 sensitivity of the transcription factor FNR is controlled by Ser24 modulating the kinetics of [4Fe-4S] to [2Fe-2S] conversion. *Proc Natl Acad Sci USA* 106:4659–4664.
29. Smith AD, et al. (2001) Sulfur transfer from IscS to IscU: The first step in iron-sulfur cluster biosynthesis. *J Am Chem Soc* 123:11103–11104.
30. Crack J, Green J, Thomson AJ (2004) Mechanism of oxygen sensing by the bacterial transcription factor fumarate-nitrate reduction (FNR). *J Biol Chem* 279:9278–9286.
31. Lee Y, et al. (2016) A [3Fe-3S](3+) cluster with exclusively μ-sulfide donors. *Chem Commun (Camb)* 52:1174–1177.
32. Sanakis Y, et al. (2000) Evidence for antisymmetric exchange in cuboidal $[3Fe\text{-}4S]^{+}$ clusters. *J Am Chem Soc* 122:11855–11863.
33. Crack JC, Green J, Thomson AJ, Le Brun NE (2014) Techniques for the production, isolation, and analysis of iron-sulfur proteins. *Methods Mol Biol* 1122:33–48.
34. Laganowsky A, Reading E, Hopper JT, Robinson CV (2013) Mass spectrometry of intact membrane protein complexes. *Nat Protoc* 8:639–651.
35. Kay KL, Hamilton CJ, Le Brun NE (2016) Mass spectrometry of *B. subtilis* CopZ: Cu(i)-binding and interactions with bacillithiol. *Metallomics* 8:709–719.
36. Kuzmic P (1996) Program DYNAFIT for the analysis of enzyme kinetic data: Application to HIV proteinase. *Anal Biochem* 237:260–273.
37. Beinert H (1983) Semi-micro methods for analysis of labile sulfide and of labile sulfide plus sulfane sulfur in unusually stable iron-sulfur proteins. *Anal Biochem* 131:373–378.
38. Lanz ND, et al. (2014) Evidence for a catalytically and kinetically competent enzyme-substrate cross-linked intermediate in catalysis by lipoyl synthase. *Biochemistry* 53: 4557–4572.
39. Yu ZD, et al. (1993) The production and photodissociation of iron-sulfur cluster ions. *J Chem Phys* 99:1765–1770.